A novel antiangiogenic and vascular normalization therapy targeted against human CD160 receptor

Sophie Chabot,[1,2,3,4] Nabila Jabrane-Ferrat,[1,2,3,4] Karine Bigot,[5,6] Julie Tabiasco,[1,2,3,4] Alexandra Provost,[5,6] Muriel Golzio,[4,7] Muhammad Zaeem Noman,[8] Jérôme Giustiniani,[9,10,11] Elisabeth Bellard,[4,7] Stéphanie Brayer,[1,2,3] Maryse Aguerre-Girr,[1,2,3,4] Fabienne Meggetto,[12] Sylvie Giuriato,[12] François Malecaze,[13] Stéphane Galiacy,[13] Jean-Philippe Jaïs,[14] Olivier Chose,[15] Jean Kadouche,[15] Salem Chouaib,[8] Justin Teissié,[4,7] Marc Abitbol,[5,6] Armand Bensussan,[9,10] and Philippe Le Bouteiller[1,2,3,4]

[1]Institut National de la Santé et de la Recherche Médicale (INSERM) U1043, F-31300 Toulouse, France
[2]Centre National de la Recherche Scientifique (CNRS) U5282, F-31300 Toulouse, France
[3]Centre de Physiopathologie de Toulouse Purpan, [4]Université de Toulouse, Université Paul Sabatier (UPS), F-31300 Toulouse, France
[5]Faculté de Médecine Paris-Descartes-Site Necker, Université Paris-Descartes EA no. 2502, 75015 Paris, France
[6]Service d'Ophtalmologie, Centre Hospitalo-Universitaire Necker-Enfants-Malades, Assistance Publique-Hôpitaux de Paris, 75015 Paris, France
[7]Institut de Pharmacologie et de Biologie Structurale, CNRS, 31077 Toulouse, France
[8]Laboratoire d'immunologie des tumeurs humaines, Institut Gustave Roussy, INSERM U753, 94805 Villejuif, France
[9]Equerre Bazin, Hôpital Saint-Louis, INSERM U976, 75475 Paris Cedex 10, France
[10]Université Paris Diderot-Paris 7, 75000 Paris, France
[11]Laboratoire de thérapie cellulaire, Institut Jean Godinot, BP171 51056 Reims Cedex, France
[12]Centre de Recherches en Cancérologie de Toulouse, INSERM Unité Mixte de Recherche 1037–Université de Toulouse, UPS, F-31300 Toulouse, France
[13]Service d'Ophtalmologie, Centre Hospitalo-Universitaire Toulouse, Hôpital Purpan, Equipe Accueil Universitaire EA "GR2DE" de l'Université de Toulouse (UPS), F-31300 Toulouse, France
[14]Service de Biostastistiques et Bioinformatique, Assistance Publique-Hôpitaux de Paris, Centre Hospitalo-Universitaire Necker-Enfants-Malades, Université Paris-Descartes EA no. 4067, 75015 Paris, France
[15]Matbiopharma, 91030 Evry Cedex, France

Angiogenesis plays an essential role in several diseases of the eye and in the growth of solid tumors, but existing antiangiogenic therapies have limited benefits in several cases. We report the antiangiogenic effects of a monoclonal antibody, CL1-R2, in several animal models of neovascularization. CL1-R2 recognizes human CD160, a membrane receptor which is conserved in various mammal species. We show that CD160 is expressed on the endothelial cells of newly formed blood vessels in human colon carcinoma and mouse B16 melanoma but not in vessels of healthy tissues. CL1-R2 reduced fibroblast growth factor 2–induced neovascularization in the rabbit cornea, in a mouse model of oxygen–induced retinopathy, and in a mouse Matrigel plug assay. Treatment of B16 melanoma–bearing mice with CL1-R2 combined with cyclophosphamide chemotherapy caused regression of the tumor vasculature and normalization of the remaining vessels as shown by Doppler ultrasonography, intravital microscopy, and histology. These studies validate CD160 as a potential new target in cases of human pathological ocular and tumor neoangiogenesis that do not respond or become resistant to existing antiangiogenic drugs.

CORRESPONDENCE
Philippe le Bouteiller:
philippe.le-bouteiller@inserm.fr
OR
Nabila Jabrane-Ferrat:
nabila.jabrane-ferrat@inserm.fr

Abbreviations used: ALK, anaplastic lymphoma kinase; AMD, age-related macular degeneration; DUS, Doppler ultrasonography; FGF2, fibroblast growth factor 2; SMA, smooth muscle actin; TPM3, tropomyosin 3; VEGF, vascular endothelial growth factor.

Angiogenesis, the formation of new blood vessels from the preexisting vasculature, occurs physiologically during embryogenesis, the menstrual cycle, and wound healing (Carmeliet, 2005), but it is also important in certain pathologies, notably in ocular neovascular diseases (a leading cause of vision loss in the world; Sherris, 2007) and in tumor growth, invasion, and metastasis (Carmeliet, 2005). Tumor-induced angiogenesis is a major obstacle to successful immune therapy, as it prevents both migration of immune effector cells into established solid tumors and delivery of chemotherapeutic drugs (Buckanovich et al., 2008). Various therapies that limit angiogenesis are being pursued (Shojaei and Ferrara, 2007), including mAbs and small molecule inhibitors (Folkman, 2007; Cao, 2009; Pàez-Ribes et al., 2009; Takeda et al., 2009). Of these, mAbs used alone or in combination with other drugs have proven to be the most successful for treating ocular neovascularization and tumor growth (Ma and Adjei, 2009). Various engineered mAbs are in clinical use to block angiogenic factors such as vascular endothelial growth factor (VEGF) or VEGF receptor 2, thus abrogating VEGF signaling (Ma and Adjei, 2009). The humanized IgG1 mAb against VEGF-A, bevacizumab (Avastin), and its derivative ranibizumab (Lucentis; Genentech and Novartis), which has a smaller molecular mass and a higher affinity for VEGF, were approved by the FDA (Rosenfeld et al., 2006) as intravitreal injections for the treatment of several ocular neovascular diseases including subfoveal neovascular wet age-related macular degeneration (AMD; Rosenfeld et al., 2006), diabetic retinopathies (Fletcher and Chong, 2008), neovascular glaucoma (Duch et al., 2009; Moraczewski et al., 2009), and various corneal pathologies (Dastjerdi et al., 2009; Jacobs et al., 2009; Oh et al., 2009). To date, the benefit of this therapy for AMD patients is, at best, transient, although its prolonged use for up to 7 mo has no deleterious effects on the retina or choroids (Ueno et al., 2008). Bevacizumab was also the first FDA-approved angiogenesis inhibitor mAb for treatment of metastatic colorectal, nonsmall cell lung, and breast cancers in combination with conventional chemotherapy (Salgaller, 2003; Gerber and Ferrara, 2005; Reichert and Valge-Archer, 2007; Ellis and Hicklin, 2008; Ma and Adjei, 2009). After a period of clinical benefit, however, this mAb fails to produce an enduring clinical response in most patients as a result of adaptive resistance and compensatory mechanisms (Dorrell et al., 2007; Bergers and Hanahan, 2008). Another important limitation of this drug is that it also affects the vasculature of normal tissues leading to diverse adverse effects including risk of arterial thromboembolic events (Ratner, 2004; Chen and Cleck, 2009).

Given the evidence that resistance develops to anti-VEGF mAb therapies, there is a pressing need to develop additional and/or combined antiangiogenic therapies that inhibit pathological neovascularization while having little or no effect on normal mature tissue vasculature. We hypothesized that CD160, a glycosylphosphatidylinositol-anchored protein initially known as BY55 (Bensussan, 2000), might be an interesting antiangiogenic target in vivo for the following reasons. First, the distribution of CD160 in healthy tissues in situ is highly restricted (Anumanthan et al., 1998). We found that CD160 is expressed by growing but not quiescent endothelial cells in culture (Fons et al., 2006). Second, using in vitro assays, we have demonstrated that CL1-R2, an IgG1 mAb directed against human CD160 which recognizes both human and murine CD160 (Fig. S1), had antiangiogenic properties, inducing caspase-dependent endothelial cell apoptosis, without the need for Fc receptor–bearing cytotoxic immune cells (Fons et al., 2006). Third, the CD160 gene is not only present in the human genome but is conserved in several mammalian species, including rabbits and mice (Maeda et al., 2005; Fons et al., 2006), thus allowing in vivo experiments on these animals. In this paper, we bring the proof of principle of the in vivo antiangiogenic therapeutic efficacy of CL1-R2 in different animal models of ocular and tumor neovascularization. In mouse transplanted B16 melanoma tumors, as well as in a transplant model of anaplastic lymphoma kinase (ALK)-induced fibroblast tumors in athymic nude mice (Giuriato et al., 2007), CL1-R2 not only inhibits tumor vascular density but also normalizes the structure of the remaining vessels, allowing better delivery of a chemotherapeutic agent.

RESULTS

The CL1–R2 mAb inhibits ocular neovascularization in rabbit cornea and oxygen–induced retinopathy in a mouse model

We evaluated the antiangiogenic properties of CL1-R2 mAb in vivo by using two different ocular neoangiogenesis animal models. The vertebrate eye has an advantage for these studies in that it is considered to be an immunoprivileged site (Cursiefen, 2007), thus possibly devoid of immune cells that could bind CL1-R2. We first used a rabbit corneal pocket assay (Fons et al., 2006) to determine whether CL1-R2 inhibits fibroblast growth factor 2 (FGF2)–induced corneal neovascularization. The cornea is normally devoid of both blood and lymphatic vessels and actively maintains this avascularity (Cursiefen, 2007). In this model, neovessels are attracted from the limbus. Neovascularization was assessed 8 d after transplantation of corneal implants containing FGF2 and two subconjunctival injections of 100 μg CL1-R2 or control IgG1. Treatment with CL1-R2 significantly decreased corneal neovascularization when compared with control IgG1-treated rabbits (Fig. 1, A and B). These findings indicate that CL1-R2 treatment inhibits growth factor–induced corneal neovascularization.

Next, we investigated the effect of CL1-R2 in a mouse model of human retinopathy of prematurity by exposing premature newborn mice (postnatal day (P) 7–12) to high oxygen levels (Smith et al., 1994; Economopoulou et al., 2005). In 100% of these animals the return to normoxic conditions induced retinal ischemia and VEGF-dependent preretinal vascularization. We first performed a qualitative assessment of the retinal vasculature on flat-mounted FITC-dextran–perfused whole retinas after intravitreal injections of CL1-R2 or control IgG1 (Fig. 2 A). Retinas from normal untreated animals exhibited normal vascularization, i.e., both superficial and deep vascular layers which extended from the optic nerve to the periphery. The vessels formed a radial branching pattern
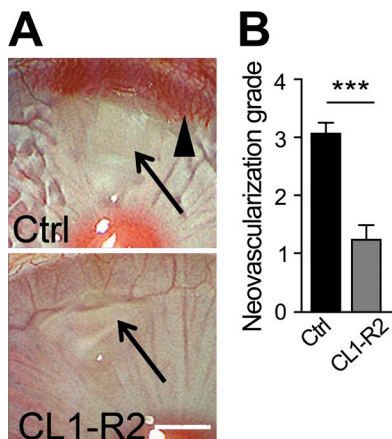
Figure 1. CL1–R2 inhibits FGF2–induced rabbit corneal neoangio-genesis. (A) Representative photographs of corneas treated with control IgG1 (Ctrl) or CL1-R2 mAb. Neovascularization was assessed 8 d after corneal grafting of FGF2-containing implants. Arrows, implants; arrow-head, neovessels. Bar, 2 mm. (B) Quantitative analysis of neovasculariza-tion in Ctrl- or CL1-R2–treated corneas. Values are means ± SEM obtained from four independent experiments, *n* = 5 rabbits/group/experiment. ***, P < 0.0001 (Mann-Whitney *U* test).

in the superficial retinal layer and a polygonal reticular pattern in the deep retinal layer. Retinas from oxygen-treated animals with no intraocular injection (Fig. 2 A, Mock) or intraocular injection of control IgG1 (Fig. 2 A, Ctrl) displayed neovascu-lar tufts that released fluorescein and had tortuous radial vessels and a central avascular zone, which is consistent with previ-ous descriptions of this model. After intraocular injection of CL1-R2, avascular areas decreased in size and the retinas con-tained fewer neovascular tufts and fewer tortuous and dilated radial vessels (Fig. 2 A), suggesting better perfusion efficiency in the central vessels.

Eyes from the various untreated or oxygen-treated ani-mals were analyzed further by histology. Serial ocular tissue sections were stained with periodic acid–Schiff reagent to visualize the nuclei of endothelial cells (Fig. 2 B). Unlike the retinas from mice in a normoxic environment (normal retina), the retinas of mock-treated mice typically contained abun-dant longitudinal and transverse aberrant microvessels of various sizes in the vitreous space and inner retina, as well as endothelial cell nuclei identified by periodic acid–Schiff staining (Fig. 2 B). Retinas from control IgG-treated animals displayed similar neovascularization with abundant aberrant microvessels and endothelial cell nuclei (Fig. 2 B). In contrast, retinas from mice injected with CL1-R2 had significantly fewer aberrant vessels, which were greatly reduced in size, especially in the vitreous space and within the retina, and fewer endothelial cell nuclei. Von Willebrand factor staining further confirmed that periodic acid–Schiff-positive cells were endo-thelial cells (Fig. 2 C). To quantify retinal neovascularization, endothelial cell nuclei and lumens of neovessels were counted in a large number of samples before and after the administration of CL1-R2 or control IgG1 (Fig. 2, D and E). These are crucial

parameters for accurately evaluating any retinal antiangio-genic effect. Intravitreal injection of CL1-R2 significantly decreased (∼35%) the mean number of endothelial cell nu-clei per section in both ganglion cell and inner nuclear layers as compared with animals injected with control IgG1 (P < 0.001; Fig. 2 D). Furthermore, CL1-R2 reduced the mean number of vessel lumens per section by ∼50% when com-pared with mock-treated (P < 0.001) or IgG1-treated control mice (P < 0.001), respectively (Fig. 2 E). We then compared the effect of CL1-R2 treatment to that of the widely used mAb bevacizumab in the same mouse model regardless of the controversy dealing with the specificity of bevacizumab to neutralize murine VEGF-A (Yu et al., 2008). Several studies have indeed conclusively demonstrated that bevacizumab, de-spite its weak affinity for the VEGF-A produced by mice, rats, guinea pigs, and rabbits, is efficient in treating experimentally induced corneal neovascularization in these animals (Bock et al., 2007; Manzano et al., 2007; Hurmeric et al., 2008; Hashemian et al., 2009; Habot-Wilner et al., 2010). Further-more, a recent study showed unambiguously that bevacizumab had a very significant inhibitory effect on retinal angiogenesis in the oxygen-induced retinopathy mouse model (Zhang et al., 2009). These latter results are in full agreement with ours. After intraocular injection of bevacizumab, we observed normalized retinal vascularization on flat-mounted retinas and retinal tissue sections comparable to that obtained after CL1-R2 treatment (Fig. S2, A and B). Quantitative analysis indicated that the mean number of endothelial cell nuclei per section was not significantly different between CL1-R2–treated and bevacizumab-treated mice (Fig. S2 C), whereas the number of vessel lumens per section was significantly lower in CL1-R2–injected mice than in bevacizumab-treated control mice (P < 0.05; Fig. S2 D). Overall, these data show that CL1-R2 mAb monotherapy efficiently suppresses path-ological angiogenesis in rabbit cornea and mice with isch-emic retinopathy.

The CL1–R2 mAb inhibits FGF2–induced vascularization in the mouse Matrigel plug assay

We then evaluated the antiangiogenic effect of CL1-R2 in vivo on the mouse Matrigel plug model of angiogenesis (Passaniti et al., 1992). This assay, in which Matrigel plugs containing FGF2 are injected subcutaneously into mouse flanks, has proven to be a relatively easy method to evaluate anti-angiogenic compounds in vivo. Initial indications of the lev-els of activity of antiangiogenic compounds can be assessed visually because of the color difference in the vascularized plugs when compared with the controls. The pale color of the plugs removed from CL1-R2–treated mice indicated little FGF2-induced vascularization over a 7-d period (Fig. 3 A, top). In contrast, the reddish color of the plugs in the control IgG1-treated mice reflected the development of dense neo-vascularization. We next compared the vessel density in CL1-R2–treated and control Matrigel plugs sections stained with the endothelial cell-specific marker isolectin B4. Representative sections are shown (Fig. 3 A, bottom). The vessels in plugs from
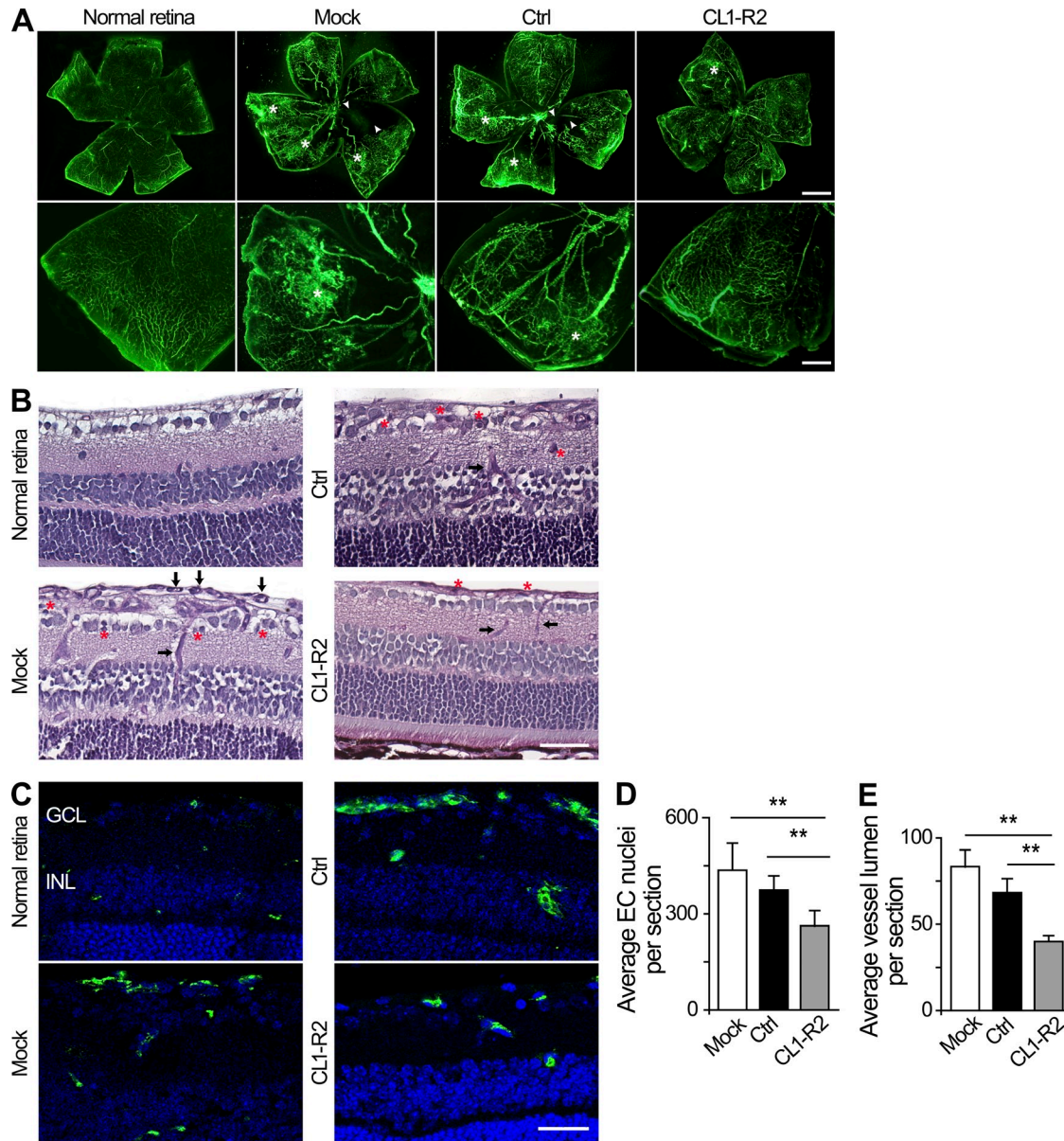
Figure 2. Intravitreal injection of CL1–R2 reduces retinal neovascularization in a murine model of oxygen–induced retinopathy. Retinal neovascularization was induced by exposing 7-d-old mice to 75 ± 2% oxygen for 5 d, and then to normoxia. Animals were injected intravitreally with control IgG1 or CL1-R2 or received no injection. (A) Flat-mounted retinas harvested from 17-d-old pups were perfused with FITC-dextran and observed by fluorescence microscopy to assess retinal vasculature. Representative flat-mounted retinas are from normal mice (Normal retina), mice exposed to hyperoxic conditions without injection (Mock), or mice injected intravitreally with 5 µg IgG1 (Ctrl) or 5 µg CL1-R2. Central avascular zone, arrowheads; neovascular tufts, asterisks. Data are representative of three independent experiments (n = 6–11 mice/group). Bars: (top) 770 µm; (bottom) 335 µm. (B) Histological analyses (periodic acid–Schiff staining) of whole eye tissue sections. Representative photomicrographs of eye sections from normal mice (Normal retina; n = 3) and mice exposed to hyperoxic conditions without injection (Mock; n = 6) or injected intravitreally with IgG1 (Ctrl; n = 9) or CL1-R2 (n = 11). Longitudinal and transverse aberrant microvessels, arrows; isolated nuclei of endothelial cells not involved in tube formation, asterisks. GCL, ganglion cell layer; INL, inner nuclear layer. Bar, 50 µm. (C) Von Willebrand Factor staining of whole eye tissue sections. Representative photomicrographs of eye sections from normal mice (Normal retina) and mice exposed to hyperoxic conditions without injection (Mock) or injected intravitreally with IgG1 (Ctrl) or CL1-R2 mAb. After paraffin removal, sections were rehydrated, treated with 0.3% Triton X-100, and incubated with polyclonal antibody against Von Willebrand factor, followed by Alexa Fluor 488 secondary antibody (green) and counterstaining with DAPI (blue). GCL, ganglion cell layer; INL, inner nuclear layer. Bar, 25 µm. (D and E). Quantitative assessment of the retinal vascularization illustrated in B for 6 (Mock), 9 (Ctrl), or 11 (CL1-R2) mice/group. Endothelial cell nuclei and vessel lumens were counted on four to eight sections per eye stained with periodic acid–Schiff reagent. The mean number of endothelial cell (EC) nuclei (D) and vessel lumen (E) presented in the histograms were determined using a Poisson regression model for clustered data. 95% confidence intervals of the mean number estimates are figured as error bars. P-values were corrected for post-hoc group comparisons by the Bonferroni method. **, P < 0.001.

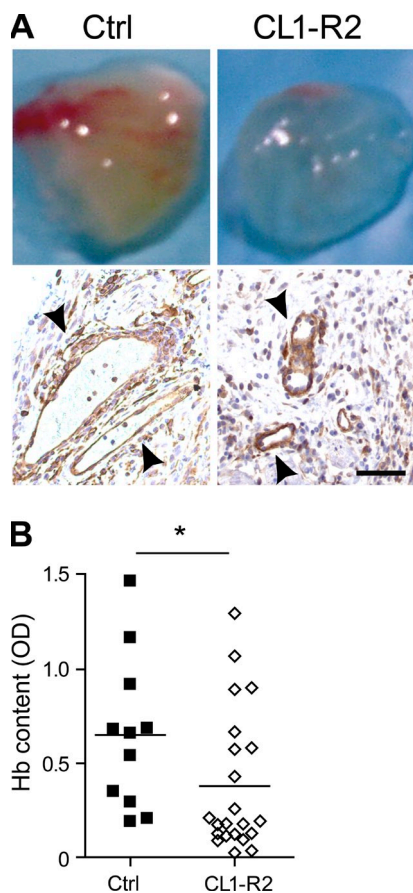**Figure 3. CL1–R2 inhibits FGF2–induced neoangiogenesis in a Matrigel plug model.** (A, Top) Photographs of representative FGF2-containing Matrigel plugs taken from control IgG1- and CL1-R2–treated mice 7 d after plug implantation. (A, Bottom) Representative sections of FGF2-containing Matrigel plugs taken from control IgG1- and CL1-R2–treated mice on day 7. Endothelial cells were labeled with isolectin B4 (brown) and the sections were counterstained with hematoxylin (blue). Arrowheads indicate isolectin B4-positive vessels. Bar, 50 µm. Representative images of five independent experiments. (B) Quantification of hemoglobin in FGF2-containing Matrigel plugs removed from control IgG1- and CL1-R2–treated mice. Horizontal bars represent the mean hemoglobin content. n = 11 IgG1-treated mice; n = 22 CL1-R2–treated mice. *, P = 0.0153 (Mann-Whitney U test). Pooled data are from five independent experiments.

CL1-R2–treated animals were smaller and fewer in number than those in plugs from the control mice. We quantified the level of angiogenesis by determining the hemoglobin content of the plugs and found a marked reduction (~45%, P = 0.0153) in plugs from CL1-R2–treated mice when compared with those from IgG1-treated control mice (Fig. 3 B). In 14 out of 22 CL1-R2–treated Matrigel plugs, the hemoglobin content was extremely low. These data indicate that the CL1-R2 mAb significantly impaired angiogenesis in this in vivo assay.

Treatment with the CL1–R2 mAb inhibits transplanted murine B16 vascular density
To further evaluate the antiangiogenic activity of CL1-R2 in vivo, we used the transplanted mouse B16 melanoma tumor model,

which is poorly immunogenic and highly vascularized. Histological analysis of these tumors showed that the vascularization was significantly lower in CL1-R2–treated mice than in control animals (Fig. 4, A and B; P = 0.0001). Histology gave an instantaneous picture of vascularization but did not reflect the functionality of blood vessels. So we used another approach based on the use of color Doppler ultrasonography (DUS), a noninvasive method of visualizing tumor vessels in situ at different times (Asselin-Paturel et al., 1999). DUS demonstrated that the vascular density of B16 tumors at 12, 15, and 18 d after CL1-R2 injections was significantly lower than that of tumors in control mice that received IgG1 injections (Fig. 4, C and D; and Videos 1 and 2). As B16 tumor cells are sensitive to cyclophosphamide (Hamano et al., 2004), we also investigated whether the observed vascular changes after CL1-R2 treatment increased susceptibility to this cytotoxic agent. The combination of both mAb and chemotherapeutic agent, administered according to a metronomic schedule, significantly reduced the growth of B16 tumor (Fig. 4 E; P = 0.0001) compared with control IgG1 with cyclophosphamide. Thus, CL1-R2 and cyclophosphamide act in concert to reduce neovascularization and slow the growth of B16 tumor.

Treatment with the CL1–R2 mAb normalizes the remaining vasculature of B16 tumors
The normalization of tumor vasculature with antiangiogenic therapy is an emerging concept (Jain, 2005). This vascular normalization implies that any antiangiogenic strategy should target immature dysfunctional vessels and fortify those remaining. To investigate the effect of CL1-R2 on tumor normalization, we used intravital microscopy. This method allows the continuous noninvasive analysis of the same tumor area in its orthotopic environment (in a dorsal skin-fold chamber) over a 2-wk period, including measurement of blood flow–related variables such as vessel diameter, microvascular density, and branching (Jain et al., 2002; Koehl et al., 2009). Widefield intravital fluorescence microscopy showed that CL1-R2 injections together with cyclophosphamide significantly reduced B16 tumor growth over a 14-d period after tumor implantation when compared with IgG1-treated control mice with cyclophosphamide (not depicted), confirming results obtained by caliper measurements (Fig. 4 E). The first signs of angiogenesis, including dilation and tortuous elongation of preexisting blood vessels, were observed in the host tissues of control mice soon after melanoma implantation (Fig. 5, A and B). This phenomenon was a result of the proliferating tumor remodeling the host vessels, as no modification of the preexisting vessels was observed in the absence of a grafted tumor (Fig. S3). Treatment of mice with CL1-R2 limited host vessel dilation and tortuosity (Fig. 5 A and Fig. S4). The B16 tumors were vascularized over a substantial area in control mice, whereas the area of tumor vascularization was much smaller in CL1-R2–treated animals 12 d after implantation (Fig. 5 B). At day 14 after tumor implantation (the last day of the experiment), the vascular area of B16 tumors in CL1-R2–treated mice was 2.56-fold smaller than in control mice (Fig. 5 B).
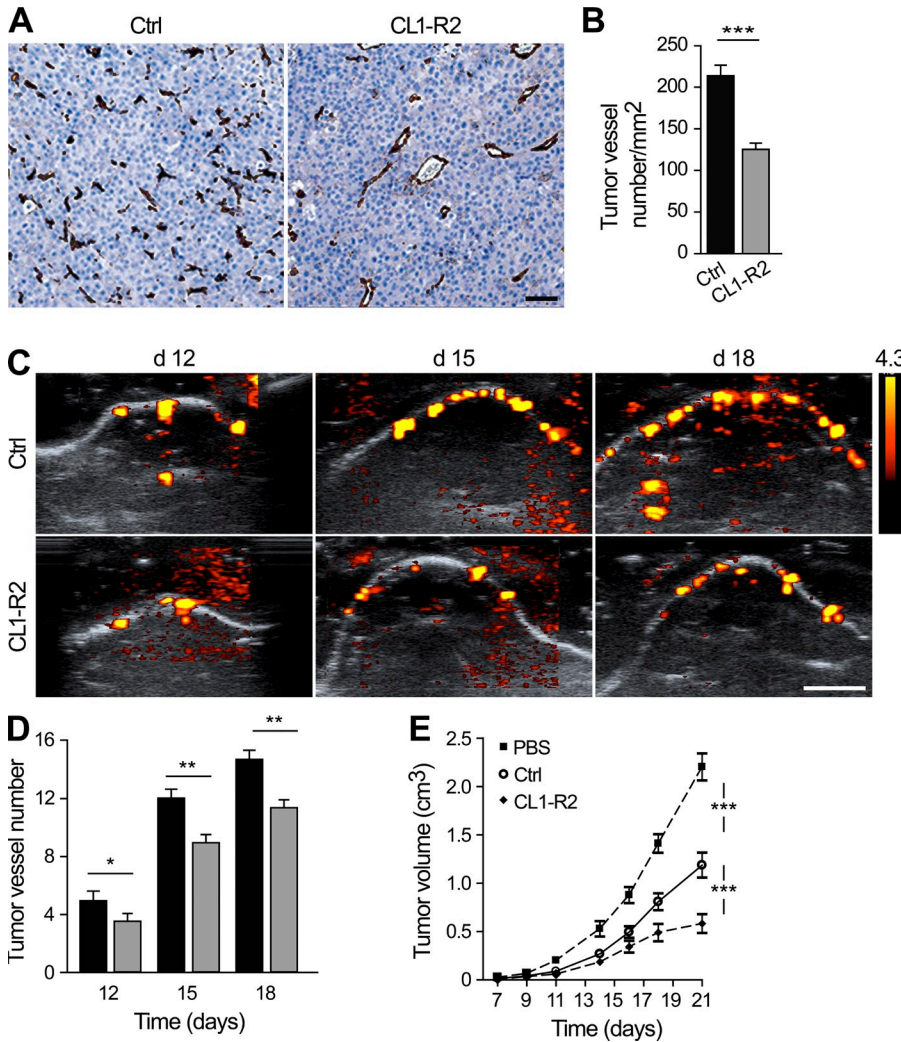
Figure 4. Diminished vascular density of B16 melanoma tumors in CL1-R2–treated mice. (A) Immunohistochemical assessment of vascular density in B16 tumor sections taken on day 16 from mice treated with control IgG1 (Ctrl) or CL1-R2, both in combination with cyclophosphamide (CycloP). Endothelial cells in representative sections were stained with isolectin B4 (brown) and counterstained with hematoxylin (blue). Images are representative of five mice in each group. Bar, 50 µm. (B) Quantification of the data shown in A. Vessel density was counted in four independent areas on each B16 tumor section. ***, P < 0.0001 (one-way ANOVA test). Error bars represent SEM. (C) 3 d after B16 cell injection, mice received repeated i.p. injections of CL1-R2 or IgG1 (Ctrl). Cyclophosphamide was then added to the drinking water. Mice were examined by DUS to identify intratumoral blood vessels 12, 15, and 18 d after the first CL1-R2 injection. Power Doppler mode color DUS ultrasound images with intratumoral blood vessel signals are shown in red/yellow. Representative images obtained from the same tumor cross section in a single mouse from day 12 to 18 are shown for each treatment. Bar, 5 mm. Side bar: Doppler power, maximum 4.3. (D) Quantification of the number of intratumoral vessels in IgG1-treated (black bars) and CL1-R2–treated (gray bars) mice determined from multiple cross sections of the tumor. Tumor vessel number on the ordinate represents the mean number of total intratumoral blood vessels per tumor because the whole tumor was scanned at each time point for the detection of blood vessels. Data are expressed as means ± SEM (n = 5 mice in each group). *, P = 0.0203 for day 12; **, P = 0.0032 for day 15; **, P = 0.0077 for day 18 (Student's t test). (E) B16 tumor growth in untreated (PBS), CL1-R2–treated (500 µg, three times a week), or control mice in combination with cyclophosphamide treatment. Tumor volumes were measured at the indicated times after tumor inoculation. Data from four experiments (n = 5 mice/group) were pooled. Data represent mean tumor size values ± SEM. ***, P < 0.0001 (two-way ANOVA test).

We then performed a fractal analysis to quantify the geometric complexity of the vascular network. This analysis offers an additional method for measuring tumor vascular damage given that tumor vasculature is characterized by loss of hierarchical architecture (Heymans et al., 2000). We found that the B16 tumor vasculature in CL1-R2–treated mice had a significantly smaller fractal dimension than in control mice (Fig. 5 C). These results indicate that treatment with CL1-R2 favored a better hierarchical architecture of the B16 tumor vessel network, which may influence the circulation. Consistent with this finding, B16 tumor vessel diameters in IgG1-treated mice varied from 2.35 to 48.33 µm, in contrast to the much more uniform tumor vessel diameters observed in CL1-R2–treated animals (6.46 to 25.94 µm; Fig. 5 D). Collectively, these observations, based on a wide range of vascular parameters, indicate that the CL1-R2 mAb, combined with cyclophosphamide chemotherapy, results in a reduced vascular density in transplanted B16 tumors and normalization of the remaining tumor vasculature when compared with IgG1-treated mice. Moreover, our data indicate that CL1-R2 treatment was effective not only if the mAb was injected on the same day as tumor cell implantation but also if injected 3 d after tumor inoculation (Fig. 4, C and D) or if a B16 tumor fragment was implanted under the skin (Fig. 5).

B16 tumor vasculature in CL1-R2–treated mice is mature and functional for chemotherapeutic drug delivery

Tumor blood vessels are immature and display functional defects, including vessel lumen collapse leading to restricted blood flow and poor access to the chemotherapeutic agents (Carmeliet, 2005; Jain, 2005; Hamzah et al., 2008). Open lumens are thus a good indicator of vessel maturation and functionality in solid tumors. By counting the vessels in different fields of each tumor section, we found that a greater proportion of B16 tumor vessels had an open lumen in CL1-R2–treated mice than in control animals (Fig. 6 A). Pericytes recruited
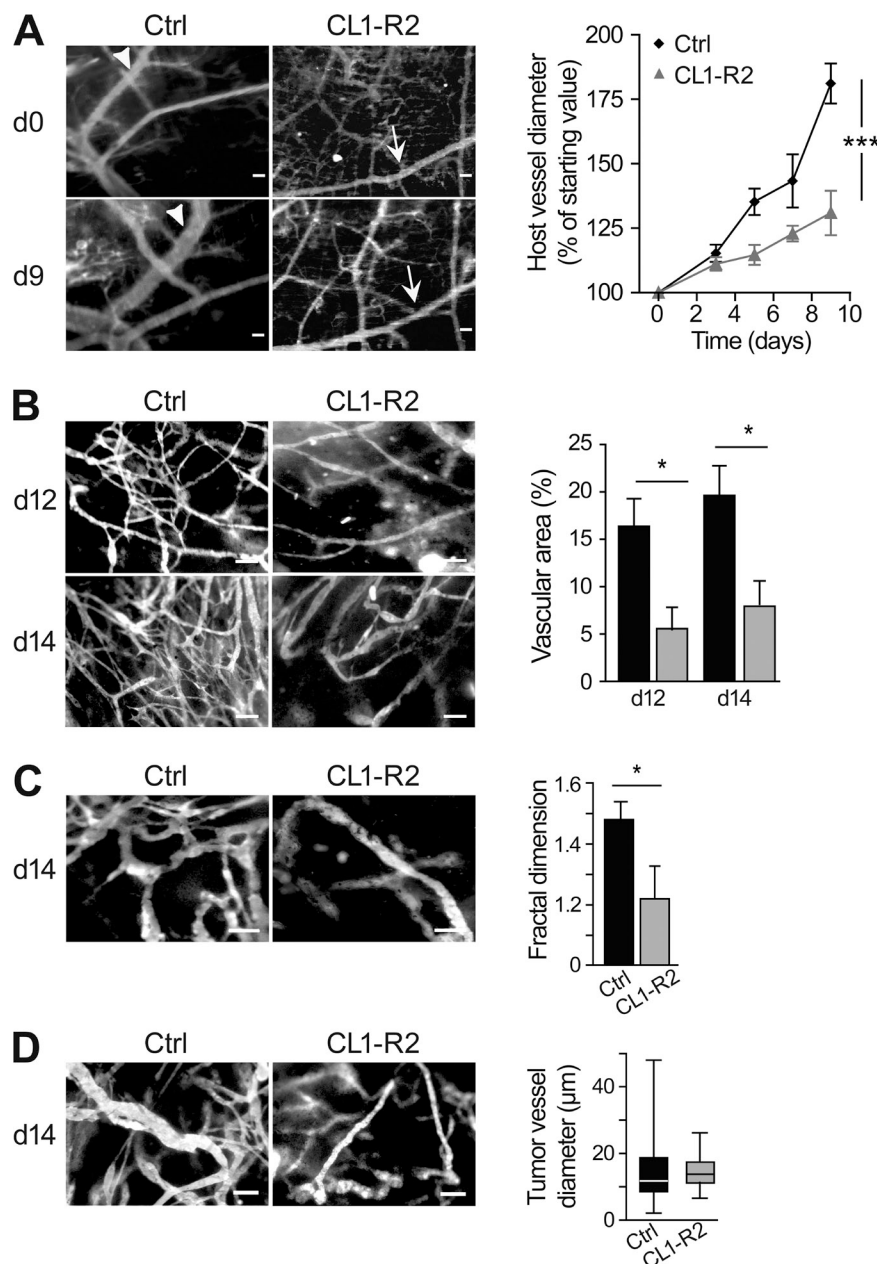
Figure 5. Normalization of B16–GFP melanoma tumor vessels in CL1–R2–treated mice observed by in vivo intravital fluorescence microscopy. (A, Left) Host vessels surrounding the tumor in control Ig or CL1–R2–treated mice in combination with cyclophosphamide at day 9 after tumor implantation. Contrast was enhanced by i.v injection of 150 kD TRITC-labeled dextran. Arrowheads and arrows point to the same tumor vessels at day 0 (d0) and day 9 (d9), respectively. Bars, 40 μm. (A, Right) Quantification of the data in the left panel. Data represent mean values ± SEM (n = 5 mice/group). ***, $P < 0.0001$ (two-way ANOVA test). (B, Left) Tumor vascular area 12 or 14 d after CL1–R2 treatment or control IgG1. Bars, 40 μm. (B, Right) Quantification of the tumor vascular areas in the left panels. Values are means ± SEM (n = 5 mice/group). *, $P = 0.0114$ (day 12); *, $P = 0.0292$ (day 14; Student's t test). (C, Left) Intratumoral microvasculature in day-14 control IgG1- or CL1–R2–treated mice. Bars, 40 μm. (C, Right) Quantitative analysis of vascular network complexity based on microvessel fractal dimension measurements in IgG1-treated (Ctrl) and CL1–R2–treated mice. Values are means ± SEM (n = 5 mice/group). *, $P = 0.0211$ (Student's t test). (D, Left) Microangiography of IgG1-treated (Ctrl) and CL1–R2–treated tumors on day 14 after implantation. Bars, 40 μm. (D, Right) Quantitative data from a representative experiment (plotted in the box/whisker format) comparing IgG1-treated (Ctrl) and CL1–R2–treated tumors on day 14 after implantation (n = 5 mice/group). Box plots show median values (horizontal line inside the whiskers box), box boundaries represent quartiles, and error bars represent the lowest and highest values. Images and quantitative data are representative of three independent experiments.

along endothelial cells are another indicator of maturation and normal functioning of blood vessels (Carmeliet, 2005). We therefore evaluated the pericyte coverage of B16 tumor vessels by confocal microscopy. The vasculature of tumors from CL1–R2–treated mice exhibited strong staining for smooth muscle actin (SMA; a marker of pericytes), unlike tumor vessels from control mice which displayed little or no staining for SMA (Fig. 6 B). These data suggested that CL1–R2–treated tumor vessels might have a lower resistance to blood flow, which may improve the blood supply within the tumor. To evaluate blood perfusion, Hoechst 33342 fluorescent dye was administered intravenously and its uptake by tumor vessels was examined by fluorescence microscopy. This dye labels the nuclei of endothelial cells and cells adjacent to the walls of perfused vessels. Little perivascular labeling was observed in B16 tumor vessels from control mice despite a high level of vascularization (Fig. 6 C). In contrast, most of the tumor vessels in CL1–R2–treated mice displayed intense perivascular staining. Thus, treatment with CL1–R2 improved perfusion efficiency in B16 tumor vessels. We next evaluated the extent to which CL1–R2 influenced tumor necrosis as a result of cyclophosphamide. Histological studies showed more extensive necrosis in CL1–R2–treated tumors than in controls (Fig. 6 D), suggesting that CL1–R2 treatment improved the delivery of cyclophosphamide by normalizing the remaining tumor blood vessels. Together, these findings demonstrated that CL1–R2 mAb treatment not only reduced abnormal tumor vasculature but also favored the maturation and function of the remaining tumor vessels.

To evaluate the therapeutic benefit of CL1–R2 mAb injection and to make a comparison with anti-VEGF mAb
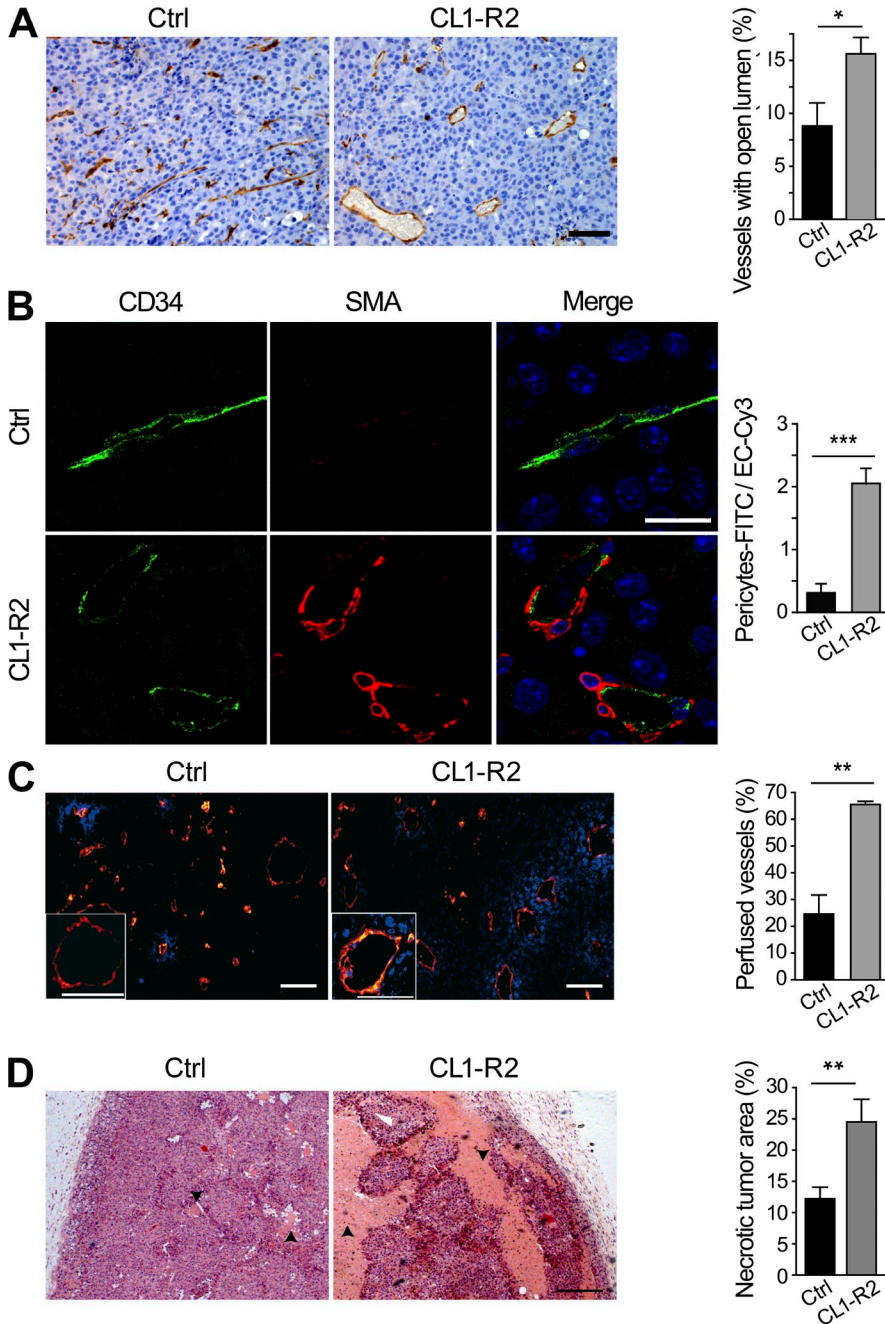
Figure 6. The B16 tumor vasculature in CL1-R2–treated mice is mature and functional. All data presented were obtained from mice 16 d after tumor implantation (A, Left) Representative B16 tumor vessels stained with isolectin B4 (brown staining; counterstaining, hematoxylin) from mice treated with CL1-R2 or control Ig in combination with cyclophosphamide. Bar, 50 µm. (A, Right) Histogram showing the number of vessels with an open lumen. Number of fields: four. $n = 5$ mice per group. *, $P = 0.0341$ (Student's t test). (B, Left) CD34-positive endothelial cells (green) are covered by SMA (red) pericyte cells in B16 tumors from CL1-R2–treated mice (bottom) compared with IgG1-treated Ctrl mice (top). Nuclei are labeled blue. Images were taken with confocal fluorescence microscopy. Bar, 20 µm. (B, Right) Quantification of the number of endothelial cells covered by pericytes. The ratio of total area red staining (SMA) to green staining (CD34) was calculated (10 fields per tumor, 5 tumors). Values are means ± SEM. ***, $P < 0.0001$. (C, Left) Cryosections of B16 tumors from control and CL1-R2–treated mice stained with isolectin B4 (red). Hoechst staining (blue) indicates perfused vessels. Insets show images at higher magnification. Bars, 50 µm. (C, Right) Quantification. $n = 5$. Number of fields: 4. **, $P = 0.0047$ (unpaired Student's t test with Welch's correction). Control = 24.59 ± 7.086 ($n = 5$); CL1-R2 = 65.52 ± 1.158 ($n = 5$). (D, Left) Histopathology of B16 tumors stained with hematoxylin and eosin. Necrosis is indicated by arrowheads. Bar, 200 µm. (D, Right) Quantification of necrotic areas in B16 tumors from CL1-R2–treated and control mice. $n = 5$ mice/group. Number of fields: 4. **, $P = 0.0092$ (Student's t test with Welch's correction). Images and quantitative data are representative of three independent experiments. The data in A, C, and D are means ± SEM of four different microscope fields for each tumor and a total of five different tumors in each treatment group.

(bevacizumab), we compared the B16 tumor burden after these different treatments combined with cyclophosphamide (Fig. S5). CL1-R2 mAb injection improved the mouse survival (35 d), compared with the earlier death (30 d) of mice injected with bevacizumab (P = 0.032) or control IgG1 (P = 0.016).

We investigated further whether CL1-R2 specifically targeted CD160 expressed by B16 tumor vessels. A representative section of B16 tumor showed intense staining of CD160 similar to that of the isolectin B4 endothelial marker (Fig. 7 A). In contrast, CD160 was barely detectable in the vessels of normal mouse heart in comparison with the strong isolectin B4 staining. We also evaluated the distribution of CD160 in

human healthy colon and colon tumors. The vessels present in colon tumors were strongly stained by CL1-R2 with patterns resembling those stained for CD31, a human endothelial cell marker (Fig. 7 B). In contrast, CL1-R2 did not stain the blood vessels present in healthy colon. As CL1-R2 recognized newly formed vessels in solid tumors but not vessels from healthy tissues, its therapeutic antiangiogenic effect is likely to be restricted to these neovessels.

DISCUSSION

Overall, our findings show that in monotherapy CL1-R2 mAb efficiently blocks pathological angiogenesis in both rabbit cornea and mice with ischemic retinopathy, whereas in combined therapy it restricts the development of abnormal B16 tumor
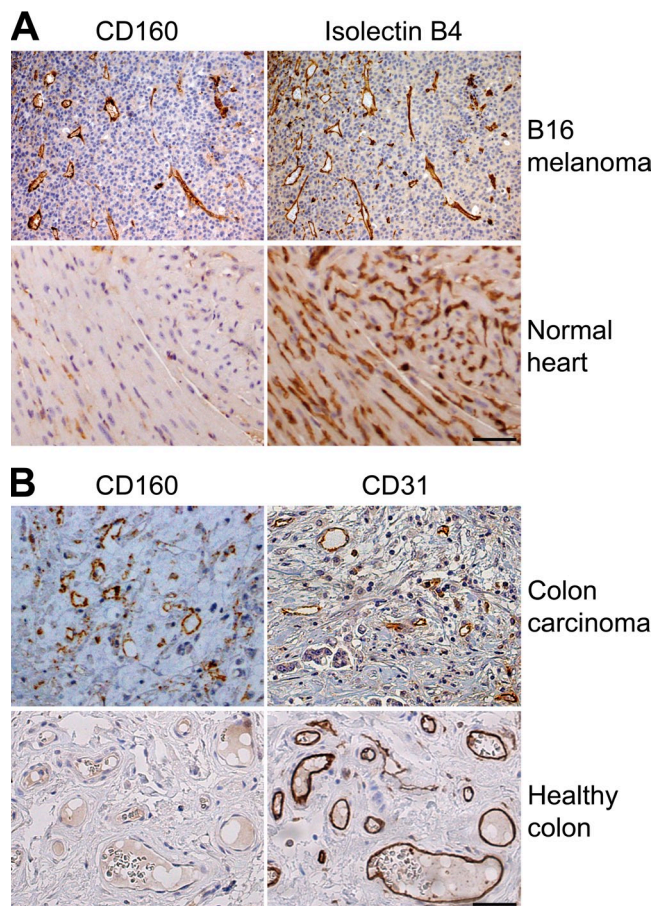
Figure 7. Expression of CD160 in tumor blood vessels but not in the blood vessels of healthy tissues. (A) Representative sections of B16 melanoma at day 16 after their subcutaneous injection (top) and healthy mouse heart (bottom), both stained with either CL1-R2 (CD160) or isolectin B4, an endothelial cell marker. Bar, 50 µm. Images are representative of four independent experiments (five mice/group). (B) Sections of human colon tumor (top) and healthy colon (bottom) stained with CL1-R2 (CD160) or a mAb against CD31, a human endothelial cell marker. Images are representative of two patient biopsies. Control IgG1 did not stain and is not shown. Bar, 50 µm.

vasculature and normalizes the remaining vessels, allowing a better delivery of a cytotoxic agent. Although CL1-R2 therapy could be used with combined angiostatic drugs that inhibit other parts of the angiogenic process (Dorrell et al., 2007; Takeda et al., 2009), our data suggest that CL1-R2 might be effective as a monotherapy for several human ocular diseases associated with neovascularization, such as diabetic retinopathy and AMD with choroidal neovascularization. These diseases remain a major cause of blindness and poor vision worldwide with an expected doubling of the prevalence of AMD in the coming decades as a result of the projected increase in the aging population.

We have previously demonstrated that, in vitro, CL1-R2 mAb inhibited FGF2-mediated tubule vessel growth from human umbilical vein endothelial cells expressing CD160 and induced their apoptosis (Fons et al., 2006). It is likely that

the CL1-R2–mediated inhibition of in vivo ocular and cancer neoangiogenesis described in this paper is the consequence of a similar caspase–dependent apoptosis mechanism. Such a mechanism differs from the existing antiangiogenic therapies targeted to VEGF/VEGFR and thus may be useful when resistance to these latter therapies occurs. We cannot exclude the possibility of a synergic antiangiogenic effect caused by both cyclophosphamide and the CL1-R2 mAb, as chemotherapeutic drugs administered with a metronomic schedule have been reported to display antiangiogenic properties (Man et al., 2002). However, this is unlikely in the B16 melanoma tumor model, as cyclophosphamide treatment alone had no effect on tumor vascular density, suggesting that CL1-R2 might be solely responsible for the antiangiogenic effect observed when combined with cyclophosphamide.

In addition to its antiangiogenic effect, we demonstrated that CL1-R2 mAb contributes to the normalization of remaining B16 vessels by producing unbranched vessels with homogeneous diameters and open lumens, resulting in a better organized network similar to the vasculature of normal tissues. Importantly, CL1-R2 treatment strongly increased the association of pericytes with the B16 tumor vasculature, demonstrating their mature status. Consistent with this, we observed in a transplant model of ALK-induced fibroblast tumors in athymic nude mice (Giuriato et al., 2007), treated with CL1-R2 mAb alone (without any combined chemotherapy), that the tumor vessels had a mature phenotype, i.e., open lumen and pericyte coverage, which is in contrast with cyclophosphamide monotherapy (Fig. S6). These latter observations made in a second tumor model confirm that CL1-R2 has a direct effect on the maturation of tumor vascularization. This property is important, as it has been shown that anti–VEGF therapy inhibited tumor vessel maturation and pericyte function (Greenberg et al., 2008). Mature vessels are more resistant to the pressure exerted by proliferating tumors, favoring drug delivery within the tumor (Padera et al., 2004). This should be the case for B16 tumors treated with CL1-R2 mAb, as we observed extensive intratumor necrosis. Moreover, it has been recently shown that the level of vessel maturation significantly contributed to the response toward antiangiogenic therapy in melanoma (Helfrich et al., 2010). Thus, CL1-R2 induced normalization of B16 tumor vessels, leading to the establishment of a stable and functional vessel network. It was shown that antiangiogenic drugs could generate a normalization window for improved delivery of chemotherapeutic drugs (Lin and Sessa, 2004). Because we gave cyclophosphamide at the same time as CL1-R2 mAb, i.e., from day 0 of B16 tumor implantation, it is very unlikely that a normalization window occurred in our tumor model. For the same reason, it is also unlikely that B16 tumors acquired an invasive and metastatic phenotype after CL1-R2 treatment, as has been recently described in other mouse tumor models (Pàez-Ribes et al., 2009). Normalization by CL1-R2 treatment of retinal vascularization in mice with ischemic retinopathy was also observed by ex vivo angiography (Fig. 2 A). These results suggest that the antiangiogenic and normalization effects are not mutually exclusive.

CL1–R2 is a bifunctional mAb, as it blocks neoangiogenesis, normalizing the remaining tumor vessels (this study), but may also activate the innate immune system (Le Bouteiller et al., 2002; Barakonyi et al., 2004). Although we did not investigate whether CL1-R2 mAb therapy activated NK cells, this possibility cannot be excluded as we previously demonstrated that specific binding of CL1-R2 mAb to CD160 on human peripheral blood NK cells triggered interferon-γ, TNF, and IL-6 production, which participated in the inflammatory response (Barakonyi et al., 2004). Activation of NK cells by CL1-R2 may thus contribute to slowing tumor growth in addition to the antiangiogenic and normalization effects of the mAb. In contrast, in cornea or retina such CL1-R2–mediated NK cell activation is unlikely, as these cells are generally not present in these tissues (Ambati et al., 2006).

In summary, we have demonstrated that the CL1-R2 mAb exerts an antiangiogenic effect on tumors in vivo; by normalizing the vasculature, it thus improves perfusion and enhances the accessibility of the tumor to chemotherapeutic drugs. These studies indicate that targeting the CD160 receptor with a specific mAb, CL1-R2, is a promising therapeutic option that could be used in monotherapy or combination therapy for the treatment of many diseases with associated pathological neovascularization. The spectrum of neovascular diseases that could be treated is potentially large, including several vision-threatening eye diseases and many solid tumors associated with high levels of angiogenesis. CL1-R2 monotherapy might be particularly apt for treatment of ocular neovascular diseases in humans, as this mAb has antiangiogenic activity alone in animal models of both corneal and retina neoangiogenesis. In combination with intravenous chemotherapy, CL1-R2 might be useful for highly vascularized cancers as this mAb also triggers vessel normalization, opening the way to a successful chemotherapy. Further investigations are ongoing to ascertain the appropriate CL1-R2 mAb dosing regimens, best route of delivery, and duration of therapy to manage the toxicities and risks of systemic exposure and to select the most effective humanized mAbs with the lowest level of immunogenicity that may be successful for treating ocular neovascular diseases and cancer (Cao and Langer, 2010).

MATERIALS AND METHODS

Murine anti–human CD160 CL1-R2 mAb. The mouse anti-CD160 CL1-R2 mAb (IgG1) was developed in our laboratory and was evaluated as an anti-CD160 mAb during the seventh Human Leukocyte Differentiation Antigen Workshop (Bensussan, 2000). We produced the CL1-R2 mAb from a specific secreting hybridoma cell line by using the high cell density system CELLine (Valdea Biosciences). The endotoxin unit concentration was <0.6 EU/mg of IgG. The mouse IgG1 isotype control monoclonal antibody He6 was developed by immunizing mice with hepatitis B surface antigen. Both CL1-R2 and IgG1 isotype control were similarly purified by affinity chromatography on a HiTrap protein G column (GE Healthcare) in an ÄKTA purifier system (GE Healthcare), dialyzed against PBS, pH 7.0, concentrated, and filtered through 0.22-µm filters. The cross-reactivity of CL1-R2 mAb with CD160 mouse proteins has been demonstrated by different means (Fig. S1): (1) using flow cytometry, we found that CL1-R2 stained mouse SVR endothelial cells as well as the BCL-1 mouse B cell chronic lymphocytic leukemia cell line (Fig. S1 A); (2) using immunoprecipitation and Western

blotting, we found that the CNX46-3 anti–mouse CD160 mAb (Cedarlane laboratories) immunoprecipitated protein bands from mouse spleen or BCL-1 cells that were blotted by the CL1-R2 mAb (Fig. S1 B); and (3) five CD160 amino acids were identified by mass spectrometry in the CNX43-6–immunoprecipitated 37-kD band blotted with CL1-R2 mAb with a minimum coverage of 37.5% (Fig. S1 C).

Animals. We used BALB/c, C57BL/6J, and NMRI-nu (nu/nu) Nude mice (Janvier Laboratories). Mice were 7–10 wk old, except for those used for the ischemic retinopathy experiments which were 7 d old. Animals were housed in a conventional temperature-controlled room (21°C), exposed to a daily 12-h period of light and dark, and fed ad libitum with a balanced diet as determined by The Jackson Laboratory for the C57BL6/J mouse strain. We used male New Zealand albino rabbits from Institut National de la Recherche Agronomique (Castanet-Tolosan). For the mouse retina experiments, animals were handled according to the guidelines of the institutional animal care committee, using protocols approved by the Ethics Committee and the ARVO Statement for use of Animals in Ophthalmic and Vision Research. All other animal experiments were performed in agreement with the European Union guidelines and the Midi-Pyrénées Ethic Committee for the care and use of laboratory animals (MP/02/37/06/08).

In vivo rabbit corneal angiogenesis assay. The corneal pocket assay used in this study has been previously described (Fons et al., 2006). We made an incision in the upper side of the cornea, 2 mm from the limbus in anesthetized rabbits. FGF2-treated implants (500 ng; R&D Systems) were inserted into this pocket. Subconjunctival injections of CL1-R2 mAb or control IgG1 (100 µg in 30 µl PBS) were administered to the upper side of the limbus 24 and 72 h after corneal implantation. Corneal neovascularization was measured 8 d after implantation and was scored on a four-grade scale based on the length of the newly formed vessels from the limbus to the FGF2-containing implant (Fons et al., 2006).

Murine model of oxygen–induced retinopathy and intravitreal injections. Retinal neovascularization was induced in mouse C57BL/6J pups using a well established and reproducible model of oxygen–induced retinopathy (Smith et al., 1994). In brief, mice (7 d old, P7) and their nursing mothers were placed in an airtight incubator and exposed to a $75 \pm 2\%$ oxygen atmosphere for 5 d. The oxygen level was continuously monitored with an oxygen analyzer (model 110; PROOX; BioSpherix). Mice were removed on P12 and maintained in normoxic conditions (room air) until P17. Mice were injected intravitreally under an operating microscope. With the exception of the non-injected group, each pup received an intravitreal injection in their left and right eyes on P12. In brief, mouse pups were anesthetized with an intramuscular injection of ketamine (100 mg/kg body weight) and xylazine (10 mg/kg body weight). The palpebral fissures were opened with microscissors and pupils were dilated with topical 10% phenylephrine and 0.5% tropicamide. The tip of a 10-mm 33-gauge steel needle, mounted on a 5-µl Hamilton syringe, was pushed through the sclera, 1 mm posterior to the corneoscleral limbus, into the vitreous body. Approximately 1 µl CL1-R2 mAb (5 µg/µl), bevacizumab (25 µg/µl; Roche), or IgG1 isotype control mAb (5 µg/µl) was injected into the vitreous cavity.

Qualitative and quantitative assessment of retinal neovascularization. Mice were killed at P17 to analyze neovascularization by histology and quantitative measurements. Some mice underwent retinal angiography with fluorescein-dextran. For this qualitative assessment, we anesthetized mouse pups as previously described and perfused the heart through the left ventricle with 1 ml PBS containing 50 mg/ml fluorescein-labeled dextran (2×10^6 mean molecular weight; Sigma-Aldrich) that had been cleared by centrifugation for 5 min at 10,000 rpm. The eyes were enucleated and fixed in 4% paraformaldehyde for 3 h. The cornea and lens were removed and the retina was dissected from the eyecup. The retina was cut into four quadrants and flat mounted in Vectashield under a coverslip for examination by fluorescence microscopy. At least 12 eyes from each treatment were examined. For the histological analysis,

mouse pups were killed and their eyes enucleated, fixed in 4% paraformaldehyde for at least 16 h at 4°C, and embedded in paraffin. We prepared sagittal 5-µm sections with a microtome (HM355, MICROM MICROTEC), stained sections with periodic acid–Schiff reagent, and counterstained with hematoxylin and eosin. We counted five to eight sections on each side of the optic nerve. Two trained investigators blindly counted the number of neovascular endothelial cells and vessel lumens across the entire retinal sample in each intact section at 100× magnification. Mean numbers of endothelial cell nuclei and vessel numbers were determined using a Poisson regression model for clustered data. 95% confidence intervals of the mean number estimates are figured as error bars. P-values were corrected for post-hoc group comparisons by the Bonferroni method. Endothelial cell–specific staining was performed by immunohistofluorescence. Paraffin was removed and sections were rehydrated and incubated for 20 min in 1× citrate buffer in a microwave at 500 W. Sections were treated with 0.3% Triton X-100 for 5 min and then incubated overnight with polyclonal antibody raised against Von Willebrand Factor at a 1:500 dilution (Abcam). Negative control immunohistochemical experiments were systematically performed with the exclusive omission of primary antibody. Sections were then incubated for 2 h at room temperature with a secondary Alexa Fluor 488 anti–sheep antibody at a 1:300 dilution (Invitrogen). After counterstaining for 10 min with DAPI at a 1:1,000 dilution (Sigma-Aldrich), washed sections were mounted in Fluorescent Mounting Medium (Dako). Optically sectioned images were acquired by confocal laser-scanning microscopy (LSM 700; Carl Zeiss).

In vivo Matrigel plug angiogenesis assays. 500-µl Matrigel plugs (BD), supplemented with 600 ng/ml FGF2 (R & D Systems) and 25 µg of either CL1-R2 mAb or an IgG1 isotype control, were injected subcutaneously into the two flanks of BALB/c mice. Every other day, 200 µg CL1-R2 mAb or IgG1 mAb was injected in vivo directly into the Matrigel plug through the skin. 7 d after injection, the animals were killed, the plugs removed, and their hemoglobin concentration evaluated sing Drabkin's reagent kit (Sigma-Aldrich). For histological analyses, Matrigel plugs were fixed in 4% paraformaldehyde and embedded in paraffin. Sections were stained by incubation with biotinylated isolectin B4 (Vector Laboratories) followed by streptavidin-peroxidase and DAB substrate.

B16 tumor model and treatment schedule. Mouse B16 tumor cells expressing GFP (a gift from J. Di Santo [Institut Pasteur, Paris] and B. Couderc [Institut National de la Santé et de la Recherche Médicale U563, Toulouse, France]) were injected subcutaneously into the flanks of C57BL/6 mice (10^5 cells per mouse). These mice received i.p. injections of 500 µg CL1-R2 mAb or IgG1 control or an equivalent volume (100 µl) of PBS three times per week starting on the day of tumor inoculation. Mice were also treated with 10 mg/kg body weight of cyclophosphamide (Sigma-Aldrich) administered daily in the drinking water. No apparent signs of toxicity, such as weight loss or lethargy, were observed in response to treatment. Tumor volume was determined three times per week by measurement with calipers. The volume was calculated as width^2 × length × 0.52.

Tropomyosin 3 (TPM3)–ALK MEF tumor model. Mouse MEF fibroblasts expressing the active mutant form of the nonmuscular TPM3-ALK were injected subcutaneously into nude mice as previously described (Giuriato et al., 2007). Mice were randomized in four treatment groups of five mice each that received IgG1 control, cyclophosphamide, CL1-R2, or CL1-R2 combined to cyclophosphamide (same protocol and doses as the B16 tumor model described in the previous section). Treatments were stated the same day as tumor implantation. Growing tumors were harvested 21 d later, fixed, and paraffin embedded for subsequent immunohistochemical or confocal microscopy analysis.

Dorsal skin-fold chamber model and intravital microscopy. The experimental protocol was similar to that used in previous studies (Makale, 2007). C57BL/6 mice were anesthetized, and then a double layer of skin was sandwiched between two titanium frames and a layer of skin was surgically removed to create an observation window that was then covered with a glass coverslip with a 12-mm diameter. At the end of the surgery and the day after,

mice received an intramuscular injection of 10 mg/kg ketoprofen (50 µl in each thigh) to prevent inflammation. After implantation, C57/Bl6 mice were housed individually and allowed to recover for 1 d. We temporarily removed the coverslip and deposited a B16-GFP tumor fragment (∼1-mm diameter) in the middle of the chamber. Mice tolerated the skin-fold chamber well and showed no signs of discomfort or changes in sleeping and feeding behavior. Mice were given an i.p. injection of 500 µg CL1-R2 or IgG1 control three times per week together with 10 mg/kg cyclophosphamide administered in the drinking water. Animals anesthetized with 2% isoflurane were analyzed by intravital microscopy on days 0, 2, 5, 7, 9, 12, and 14 after the tumors were implanted. These observations were performed with a MacroFluo microscope (Leica) equipped with wide-field objectives (Plan apo 2× for Z6/Z16 with 0.57×, 2×, and 4× objectives) and a cooled charge-coupled device camera (CoolSNAP HQ; Roper Scientific). Fluorescence excitation was obtained with a Mercury arc lamp (HBO; Osram) and a GFP filter (Leica). We used MetaVue software (Molecular Devices) for image acquisition. 50 µl of 0.5% tetramethylrhodamine isothiocyanate–labeled dextran (TRITC-dextran; Sigma-Aldrich) in PBS was injected intravenously to obtain better contrast when viewing vessels. To calculate the tumor area, mean vessel diameter, vascular area, and microvessel fractal dimension, digital images were obtained from up to five locations within the tumor and analyzed with ImageJ software (1.36b; National Institutes of Health). By applying a Gaussian Blur filter and threshold, nonspecific pixels were removed, blood vessels were identified, and vascular areas were calculated. The binary images were reduced to a 1-pixel-wide skeleton. We calculated the microvessel fractal dimension with the FracLac v2.4e plug-in, available in the Image J environment, using the box-counting method. The image was divided into increasingly smaller boxes and the number of boxes of size ε required to cover the vasculature was counted and indicated as N(ε). Fractal dimension was calculated and indicated as N(ε). Fractal dimension (Df) is given by: $Df = \lim_{\varepsilon \to 0}[\log N(\varepsilon)/\log(\varepsilon)]$.

DUS analysis. C57/BL6 mice were injected subcutaneously with 10^5 B16 cells and treated 3 d later with i.p. injections (three times per week) of 500 µg of either CL1-R2 or control IgG. Cyclophosphamide was added to the drinking water. We analyzed changes in the number of intratumoral blood vessels by carrying out DUS analysis on days 12, 15, and 18 after the first CL1-R2 injection, as previously described (Elie et al., 2007). In brief, mice were anesthetized 15 min before each DUS analysis by an i.p. injection of 0.2 ml of a mixture of 10 mg/ml ketamine (Pfizer) and 0.1% xylazine (Bayer). One group of mice received repeated i.p. injections of 500 µg CL1-R2 mAb, whereas another group received IgG1 control antibody (five mice per group). We performed examinations with a diagnostic ultrasound system (Aplio SSA-770A; Toshiba) with two high-frequency large-bandwidth probes: 9 MHz (PZT-PLT 604AT; Toshiba) and 14 MHz (PZT-PLT1204AT; Toshiba). We optimized the sonograph settings for small and superficial tumors, and these settings remained unchanged for all examinations. We used a 50.0-mm Eko-Gel high polymer ultrasound standoff pad (Eurocamina SRL) between the transducer and the tumor surface. Color DUS scans were performed in the power Doppler mode for evaluation of the number of blood vessels within tumors. We determined the number of vessels for multiple cross sections of the tumor.

Histopathology and immunostaining. Human normal or adenocarcinoma colon biopsies were obtained from P. Brousset (Laboratory of Anatomy and Pathological Cytology, Purpan Hospital, Toulouse, France). Grafted Matrigel plugs, B16 tumors at day 16, or human colon biopsies specimens were fixed in 4% paraformaldehyde and embedded in paraffin. Mouse vessels were stained with the biotinylated isolectin B4 (Vector Laboratories) at 1:200 dilutions and human vessels with the mouse anti-CD31 antibody (Dako) at 1:200 dilutions, followed by biotinylated rat anti–mouse secondary antibody (BD). Immune complexes were visualized using the VECTASTAIN Elite ABC system (Vector Laboratories). For CD160 visualization, tumor sections were stained with 6 µg/ml of the CL1-R2 anti–CD160 mAb and incubated with the TSA tyramide amplification kit (Dako) according to the manufacturer's instructions. For necrosis analysis, B16 tumors sections were stained with hematoxylin and eosin. In perfusion experiments, mice received an i.v. injection of 40 mg/kg of the fluorescent DNA-binding dye Hoechst

33342 (Sigma-Aldrich) 1 min before killing. Tumors were removed and immediately frozen in liquid nitrogen. Frozen tissue sections were stored in the dark at −80°C. Labeled vessels were viewed under a microscope using 350-nm excitation filters to observe the blue fluorescence. Vessels were stained with biotinylated isolectin B4 (Vector Laboratories) at a 1:10 dilution, followed by streptavidin-phycoerythrin (1:100 dilution; Dako). For confocal microscopy, paraffin-embedded sections were stained with 2 µg/ml of rabbit anti-SMA (Spring Bioscience) or rat anti-CD34 (2 µg/ml; AbD Serotec), followed by anti–rabbit or anti–rat antibodies conjugated with Alexa Fluor 543 or Alexa Fluor 488 (Invitrogen). Nuclei were counterstained with DAPI. Slides were analyzed using a confocal microscope (LSM 710; Carl Zeiss).

Statistics. For the mouse and rabbit model experiments, quantitative data (presented as mean ± SEM) were analyzed with Prism 4 or Prism 5 (Graph-Pad Software). A mean value for each vascular variable (intravital microscopy and histological analysis) was determined for each animal, and these values were used to calculate the overall mean for all the animals in each experimental group. Before carrying out statistical tests, we determined whether the data were normally distributed and evaluated their variance. We then performed the appropriate tests as indicated. For in vivo time course experiments, we used two-way ANOVA analysis or Student's t test. We report the actual p-value for each test. $P < 0.05$ was considered statistically significant. For the retina counts, because there are two nested levels of dependence between histological sections pertaining to the same eye and the same mouse, counts of cell nuclei and vessel lumens were analyzed by a Poisson generalized linear mixed model (Wolfinger and O'Connell, 1993) with proc GLIM-MIX of the SAS statistical package v9.1.3 (Sas Institute). We considered experimental treatment groups as fixed effect factors and individual eyes as random effects. At the upper limit, robust empirical variance of the fixed effect estimates (Liang and Zeger, 1986) was computed by defining the mice as clusters. $P < 0.05$ was considered statistically significant.

Online supplemental material. Fig. S1 shows that CL1-R2 mAb cross reacts with mouse CD160, using immunoprecipitation, Western blotting, and mass spectrometry analysis. Fig. S2 compares the effects of intravitreal injection of CL1-R2 and bevacizumab on retinal neovascularization in a mouse model of oxygen–induced retinopathy. Fig. S3 shows that dilation of preexisting host vessels does not occur in the absence of grafted B16 tumor. Fig. S4 shows that CL1-R2 treatment inhibits tumor-induced host vessels dilation. Fig. S5 shows that CL1-R2 injection improves the B16 tumor-bearing mouse survival when compared with bevacizumab treatment. Fig. S6 shows that CL1-R2 treatment induces vessel maturation in transplanted TPM3-ALK MEF tumor. Online supplemental material is available at http://www.jem.org/cgi/content/full/jem.20100810/DC1.

REFERENCES

Ambati, B.K., M. Nozaki, N. Singh, A. Takeda, P.D. Jani, T. Suthar, R.J. Albuquerque, E. Richter, E. Sakurai, M.T. Newcomb, et al. 2006. Corneal avascularity is due to soluble VEGF receptor-1. *Nature.* 443:993–997. doi:10.1038/nature05249

Anumanthan, A., A. Bensussan, L. Boumsell, A.D. Christ, R.S. Blumberg, S.D. Voss, A.T. Patel, M.J. Robertson, L.M. Nadler, and G.J. Freeman. 1998. Cloning of BY55, a novel Ig superfamily member expressed on NK cells, CTL, and intestinal intraepithelial lymphocytes. *J. Immunol.* 161:2780–2790.

Asselin-Paturel, C., N. Lassau, J.M. Guinebretière, J. Zhang, F. Gay, F. Bex, S. Hallez, J. Leclere, P. Peronneau, F. Mami-Chouaib, and S. Chouaib. 1999. Transfer of the murine interleukin-12 gene in vivo by a Semliki Forest virus vector induces B16 tumor regression through inhibition of tumor blood vessel formation monitored by Doppler ultrasonography. *Gene Ther.* 6:606–615. doi:10.1038/sj.gt.3300841

Barakonyi, A., M. Rabot, A. Marie-Cardine, M. Aguerre-Girr, B. Polgar, V. Schiavon, A. Bensussan, and P. Le Bouteiller. 2004. Cutting edge: engagement of CD160 by its HLA-C physiological ligand triggers a unique cytokine profile secretion in the cytotoxic peripheral blood NK cell subset. *J. Immunol.* 173:5349–5354.

Bensussan, A. 2000. BY55 (CD160). *Protein Rev. Web.* 1:72–73.

Bergers, G., and D. Hanahan. 2008. Modes of resistance to anti-angiogenic therapy. *Nat. Rev. Cancer.* 8:592–603. doi:10.1038/nrc2442

Bock, F., J. Onderka, T. Dietrich, B. Bachmann, F.E. Kruse, M. Paschke, G. Zahn, and C. Cursiefen. 2007. Bevacizumab as a potent inhibitor of inflammatory corneal angiogenesis and lymphangiogenesis. *Invest. Ophthalmol. Vis. Sci.* 48:2545–2552. doi:10.1167/iovs.06-0570

Buckanovich, R.J., A. Facciabene, S. Kim, F. Benencia, D. Sasaroli, K. Balint, D. Katsaros, A. O'Brien-Jenkins, P.A. Gimotty, and G. Coukos. 2008. Endothelin B receptor mediates the endothelial barrier to T cell homing to tumors and disables immune therapy. *Nat. Med.* 14:28–36. doi:10.1038/nm1699

Cao, Y. 2009. Tumor angiogenesis and molecular targets for therapy. *Front. Biosci.* 14:3962–3973. doi:10.2741/3504

Cao, Y., and R. Langer. 2010. Optimizing the delivery of cancer drugs that block angiogenesis. *Sci. Transl. Med.* 2:ps3.

Carmeliet, P. 2005. Angiogenesis in life, disease and medicine. *Nature.* 438:932–936. doi:10.1038/nature04478

Chen, H.X., and J.N. Cleck. 2009. Adverse effects of anticancer agents that target the VEGF pathway. *Nat Rev Clin Oncol.* 6:465–477. doi:10.1038/nrclinonc.2009.94

Cursiefen, C. 2007. Immune privilege and angiogenic privilege of the cornea. *Chem. Immunol. Allergy.* 92:50–57. doi:10.1159/000099253

Dastjerdi, M.H., K.M. Al-Arfaj, N. Nallasamy, P. Hamrah, U.V. Jurkunas, R. Pineda II, D. Pavan-Langston, and R. Dana. 2009. Topical bevacizumab in the treatment of corneal neovascularization: results of a prospective, open-label, noncomparative study. *Arch. Ophthalmol.* 127:381–389. doi:10.1001/archophthalmol.2009.18

Dorrell, M.I., E. Aguilar, L. Scheppke, F.H. Barnett, and M. Friedlander. 2007. Combination angiostatic therapy completely inhibits ocular and tumor angiogenesis. *Proc. Natl. Acad. Sci. USA.* 104:967–972. doi:10.1073/pnas.0607542104

Duch, S., O. Buchacra, E. Milla, D. Andreu, and J. Tellez. 2009. Intracameral bevacizumab (Avastin) for neovascular glaucoma: a pilot study in 6 patients. *J. Glaucoma.* 18:140–143. doi:10.1097/IJG.0b013e318170a747

Dufresne-Martin, G., J.F. Lemay, P. Lavigne, and K. Klarskov. 2005. Peptide mass fingerprinting by matrix-assisted laser desorption ionization mass spectrometry of proteins detected by immunostaining on nitrocellulose. *Proteomics.* 5:55–66. doi:10.1002/pmic.200400902

Economopoulou, M., K. Bdeir, D.B. Cines, F. Fogt, Y. Bdeir, J. Lubkowski, W. Lu, K.T. Preissner, H.P. Hammes, and T. Chavakis. 2005. Inhibition of pathologic retinal neovascularization by alpha-defensins. *Blood.* 106:3831–3838. doi:10.1182/blood-2005-03-0889

Elie, N., A. Kaliski, P. Péronneau, P. Opolon, A. Roche, and N. Lassau. 2007. Methodology for quantifying interactions between perfusion evaluated by DCE-US and hypoxia throughout tumor growth. *Ultrasound Med. Biol.* 33:549–560. doi:10.1016/j.ultrasmedbio.2006.09.011

Ellis, L.M., and D.J. Hicklin. 2008. VEGF-targeted therapy: mechanisms of anti-tumour activity. *Nat. Rev. Cancer.* 8:579–591. doi:10.1038/nrc2403

Fletcher, E.C., and N.V. Chong. 2008. Looking beyond Lucentis on the management of macular degeneration. *Eye (Lond.).* 22:742–750. doi:10.1038/sj.eye.6703008

Folkman, J. 2007. Angiogenesis: an organizing principle for drug discovery? *Nat. Rev. Drug Discov.* 6:273–286. doi:10.1038/nrd2115

Fons, P., S. Chabot, J.E. Cartwright, F. Lenfant, F. L'Faqihi, J. Giustiniani, J.P. Herault, G. Gueguen, F. Bono, P. Savi, et al. 2006. Soluble HLA-G1 inhibits angiogenesis through an apoptotic pathway and by direct binding to CD160 receptor expressed by endothelial cells. *Blood.* 108:2608–2615. doi:10.1182/blood-2005-12-019919

Gerber, H.P., and N. Ferrara. 2005. Pharmacology and pharmacodynamics of bevacizumab as monotherapy or in combination with cytotoxic therapy in preclinical studies. *Cancer Res.* 65:671–680.

Giuriato, S., N. Faumont, E. Bousquet, M. Foisseau, A. Bibonne, M. Moreau, T. Al Saati, D.W. Felsher, G. Delsol, and F. Meggetto. 2007. Development of a conditional bioluminescent transplant model for TPM3-ALK-induced tumorigenesis as a tool to validate ALK-dependent cancer targeted therapy. *Cancer Biol. Ther.* 6:1318–1323.

Greenberg, J.I., D.J. Shields, S.G. Barillas, L.M. Acevedo, E. Murphy, J. Huang, L. Scheppke, C. Stockmann, R.S. Johnson, N. Angle, and D.A. Cheresh. 2008. A role for VEGF as a negative regulator of pericyte function and vessel maturation. *Nature.* 456:809–813. doi:10.1038/nature07424

Habot-Wilner, Z., I.S. Barequet, Y. Ivanir, J. Moisseiev, and M. Rosner. 2010. The inhibitory effect of different concentrations of topical bevacizumab on corneal neovascularization. *Acta Ophthalmol. (Copenh.).* 88:862–867. doi:10.1111/j.1755-3768.2009.01571.x

Hamano, Y., H. Sugimoto, M.A. Soubasakos, M. Kieran, B.R. Olsen, J. Lawler, A. Sudhakar, and R. Kalluri. 2004. Thrombospondin-1 associated with tumor microenvironment contributes to low-dose cyclophosphamide-mediated endothelial cell apoptosis and tumor growth suppression. *Cancer Res.* 64:1570–1574. doi:10.1158/0008-5472.CAN-03-3126

Hamzah, J., M. Jugold, F. Kiessling, P. Rigby, M. Manzur, H.H. Marti, T. Rabie, S. Kaden, H.J. Gröne, G.J. Hämmerling, et al. 2008. Vascular normalization in Rgs5-deficient tumours promotes immune destruction. *Nature.* 453:410–414. doi:10.1038/nature06868

Hashemian, M.N., S. Moghimi, S. Kiumehr, M. Riazi, and F.A. Amoli. 2009. Prevention and treatment of corneal neovascularization: comparison of different doses of subconjunctival bevacizumab with corticosteroid in experimental rats. *Ophthalmic Res.* 42:90–95. doi:10.1159/000224783

Helfrich, I., I. Scheffrahn, S. Bartling, J. Weis, V. von Felbert, M. Middleton, M. Kato, S. Ergün, and D. Schadendorf. 2010. Resistance to antiangiogenic therapy is directed by vascular phenotype, vessel stabilization, and maturation in malignant melanoma. *J. Exp. Med.* 207:491–503. doi:10.1084/jem.20091846

Heymans, O., J. Fissette, P. Vico, S. Blacher, D. Masset, and F. Brouers. 2000. Is fractal geometry useful in medicine and biomedical sciences? *Med. Hypotheses.* 54:360–366. doi:10.1054/mehy.1999.0848

Hurmeric, V., T. Mumcuoglu, C. Erdurman, B. Kurt, O. Dagli, and A.H. Durukan. 2008. Effect of subconjunctival bevacizumab (Avastin) on experimental corneal neovascularization in guinea pigs. *Cornea.* 27:357–362. doi:10.1097/ICO.0b013e318160d019

Jacobs, D.S., M. Lim, K.G. Carrasquillo, and P. Rosenthal. 2009. Bevacizumab for corneal neovascularization. *Ophthalmology.* 116:592–593, author reply :593–594. doi:10.1016/j.ophtha.2008.10.011

Jain, R.K. 2005. Normalization of tumor vasculature: an emerging concept in antiangiogenic therapy. *Science.* 307:58–62. doi:10.1126/science.1104819

Jain, R.K., L.L. Munn, and D. Fukumura. 2002. Dissecting tumour pathophysiology using intravital microscopy. *Nat. Rev. Cancer.* 2:266–276. doi:10.1038/nrc778

Koehl, G.E., A. Gaumann, and E.K. Geissler. 2009. Intravital microscopy of tumor angiogenesis and regression in the dorsal skin fold chamber: mechanistic insights and preclinical testing of therapeutic strategies. *Clin. Exp. Metastasis.* 26:329–344. doi:10.1007/s10585-008-9234-7

Le Bouteiller, P., A. Barakonyi, J. Giustiniani, F. Lenfant, A. Marie-Cardine, M. Aguerre-Girr, M. Rabot, I. Hilgert, F. Mami-Chouaib, J. Tabiasco, et al. 2002. Engagement of CD160 receptor by HLA-C is a triggering mechanism used by circulating natural killer (NK) cells to mediate cytotoxicity. *Proc. Natl. Acad. Sci. USA.* 99:16963–16968. doi:10.1073/pnas.012681099

Liang, K.Y., and S.L. Zeger. 1986. Longitudinal data analysis using generalized linear models. *Biometrika.* 73:13–22. doi:10.1093/biomet/73.1.13

Lin, M.I., and W.C. Sessa. 2004. Antiangiogenic therapy: creating a unique "window" of opportunity. *Cancer Cell.* 6:529–531.

Ma, W.W., and A.A. Adjei. 2009. Novel agents on the horizon for cancer therapy. *CA Cancer J. Clin.* 59:111–137. doi:10.3322/caac.20003

Maeda, M., C. Carpenito, R.C. Russell, J. Dasanjh, L.L. Veinotte, H. Ohta, T. Yamamura, R. Tan, and F. Takei. 2005. Murine CD160, Ig-like receptor on NK cells and NKT cells, recognizes classical and nonclassical MHC class I and regulates NK cell activation. *J. Immunol.* 175:4426–4432.

Makale, M. 2007. Intravital imaging and cell invasion. *Methods Enzymol.* 426:375–401. doi:10.1016/S0076-6879(07)26016-1

Man, S., G. Bocci, G. Francia, S.K. Green, S. Jothy, D. Hanahan, P. Bohlen, D.J. Hicklin, G. Bergers, and R.S. Kerbel. 2002. Antitumor effects in mice of low-dose (metronomic) cyclophosphamide administered continuously through the drinking water. *Cancer Res.* 62:2731–2735.

Manzano, R.P., G.A. Peyman, P. Khan, P.E. Carvounis, M. Kivilcim, M. Ren, J.C. Lake, and P. Chévez-Barrios. 2007. Inhibition of experimental corneal neovascularisation by bevacizumab (Avastin). *Br. J. Ophthalmol.* 91:804–807. doi:10.1136/bjo.2006.107912

Moraczewski, A.L., R.K. Lee, P.F. Palmberg, P.J. Rosenfeld, and W.J. Feuer. 2009. Outcomes of treatment of neovascular glaucoma with intravitreal bevacizumab. *Br. J. Ophthalmol.* 93:589–593. doi:10.1136/bjo.2008.151472

Oh, J.Y., M.K. Kim, M.S. Shin, H.J. Lee, J.H. Lee, and W.R. Wee. 2009. The anti-inflammatory effect of subconjunctival bevacizumab on chemically burned rat corneas. *Curr. Eye Res.* 34:85–91. doi:10.1080/02713680802607740

Padera, T.P., B.R. Stoll, J.B. Tooredman, D. Capen, E. di Tomaso, and R.K. Jain. 2004. Pathology: cancer cells compress intratumour vessels. *Nature.* 427:695. doi:10.1038/427695a

Pàez-Ribes, M., E. Allen, J. Hudock, T. Takeda, H. Okuyama, F. Viñals, M. Inoue, G. Bergers, D. Hanahan, and O. Casanovas. 2009. Antiangiogenic therapy elicits malignant progression of tumors to increased local invasion and distant metastasis. *Cancer Cell.* 15:220–231. doi:10.1016/j.ccr.2009.01.027

Passaniti, A., R.M. Taylor, R. Pili, Y. Guo, P.V. Long, J.A. Haney, R.R. Pauly, D.S. Grant, and G.R. Martin. 1992. A simple, quantitative method for assessing angiogenesis and antiangiogenic agents using reconstituted basement membrane, heparin, and fibroblast growth factor. *Lab. Invest.* 67:519–528.

Ratner, M. 2004. Genentech discloses safety concerns over Avastin. *Nat. Biotechnol.* 22:1198. doi:10.1038/nbt1004-1198

Reichert, J.M., and V.E. Valge-Archer. 2007. Development trends for monoclonal antibody cancer therapeutics. *Nat. Rev. Drug Discov.* 6:349–356. doi:10.1038/nrd2241

Rosenfeld, P.J., D.M. Brown, J.S. Heier, D.S. Boyer, P.K. Kaiser, C.Y. Chung, and R.Y. Kim; MARINA Study Group. 2006. Ranibizumab for neovascular age-related macular degeneration. *N. Engl. J. Med.* 355:1419–1431. doi:10.1056/NEJMoa054481

Salgaller, M.L. 2003. Technology evaluation: bevacizumab, Genentech/Roche. *Curr. Opin. Mol. Ther.* 5:657–667.

Sherris, D. 2007. Ocular drug development—future directions. *Angiogenesis.* 10:71–76. doi:10.1007/s10456-007-9068-y

Shojaei, F., and N. Ferrara. 2007. Antiangiogenesis to treat cancer and intraocular neovascular disorders. *Lab. Invest.* 87:227–230. doi:10.1038/labinvest.3700526

Smith, L.E., E. Wesolowski, A. McLellan, S.K. Kostyk, R. D'Amato, R. Sullivan, and P.A. D'Amore. 1994. Oxygen-induced retinopathy in the mouse. *Invest. Ophthalmol. Vis. Sci.* 35:101–111.

Takeda, A., J.Z. Baffi, M.E. Kleinman, W.G. Cho, M. Nozaki, K. Yamada, H. Kaneko, R.J. Albuquerque, S. Dridi, K. Saito, et al. 2009. CCR3 is a target for age-related macular degeneration diagnosis and therapy. *Nature.* 460:225–230. doi:10.1038/nature08151

Ueno, S., M.E. Pease, D.M. Wersinger, T. Masuda, S.A. Vinores, T. Licht, D.J. Zack, H. Quigley, E. Keshet, and P.A. Campochiaro. 2008. Prolonged blockade of VEGF family members does not cause identifiable damage to retinal neurons or vessels. *J. Cell. Physiol.* 217:13–22. doi:10.1002/jcp.21445

Welch, D.R., J.E. Bisi, B.E. Miller, D. Conaway, E.A. Seftor, K.H. Yohem, L.B. Gilmore, R.E. Seftor, M. Nakajima, and M.J. Hendrix. 1991.

Characterization of a highly invasive and spontaneously metastatic human malignant melanoma cell line. *Int. J. Cancer.* 47:227–237. doi:10.1002/ijc.2910470211

Wolfinger, R., and M. O'Connell. 1993. Generalized linear mixed models a pseudo-likelihood approach. *Journal of Statistical Computation and Simulation.* 48:233–243. doi:10.1080/00949659308811554

Yu, L., X. Wu, Z. Cheng, C.V. Lee, J. LeCouter, C. Campa, G. Fuh, H. Lowman, and N. Ferrara. 2008. Interaction between bevacizumab and murine VEGF-A: a reassessment. *Invest. Ophthalmol. Vis. Sci.* 49:522–527. doi:10.1167/iovs.07-1175

Zhang, Q., J. Zhang, Y. Guan, S. Zhang, C. Zhu, G.T. Xu, and L. Wang. 2009. Suppression of retinal neovascularization by the iNOS inhibitor aminoguanidine in mice of oxygen-induced retinopathy. *Graefes Arch. Clin. Exp. Ophthalmol.* 247:919–927. doi:10.1007/s00417-009-1066-x